

Groundwater fluxes in a shallow seasonal wetland pond: The effect of bathymetric uncertainty on predicted water and solute balances

Mark A. Trigg^{a,b,*}, Peter G. Cook^b, Philip Brunner^c

^a Hydrology Group, School of Geographical Sciences, University of Bristol, University Road, Bristol BS8 1SS, UK

^b National Centre for Groundwater Research and Training (NCGRT), School of the Environment, Flinders University, GPO Box 2100, Adelaide, SA 5001, Australia

^c Institut de Géologie et d'hydrogéologie, Université de Neuchâtel, Rue Emile-Argand 11, CH-2009 Neuchâtel, Switzerland

S U M M A R Y

Article history:

Received 11 November 2013

Received in revised form 7 February 2014

Accepted 13 June 2014

Available online 27 June 2014

This manuscript was handled by Peter K. Kitanidis, Editor-in-Chief, with the assistance of Todd C. Rasmussen, Associate Editor

Keywords:

Wetland ponds

Bathymetry

Uncertainty

PEST

Solute balance

Bézier curve

The successful management of groundwater dependent shallow seasonal wetlands requires a sound understanding of groundwater fluxes. However, such fluxes are hard to quantify. Water volume and solute mass balance models can be used in order to derive an estimate of groundwater fluxes within such systems. This approach is particularly attractive, as it can be undertaken using measurable environmental variables, such as; rainfall, evaporation, pond level and salinity. Groundwater fluxes estimated from such an approach are subject to uncertainty in the measured variables as well as in the process representation and in parameters within the model. However, the shallow nature of seasonal wetland ponds means water volume and surface area can change rapidly and non-linearly with depth, requiring an accurate representation of the wetland pond bathymetry. Unfortunately, detailed bathymetry is rarely available and simplifying assumptions regarding the bathymetry have to be made. However, the implications of these assumptions are typically not quantified. We systematically quantify the uncertainty implications for eight different representations of wetland bathymetry for a shallow seasonal wetland pond in South Australia. The predictive uncertainty estimation methods provided in the Model-Independent Parameter Estimation and Uncertainty Analysis software (PEST) are used to quantify the effect of bathymetric uncertainty on the modelled fluxes. We demonstrate that bathymetry can be successfully represented within the model in a simple parametric form using a cubic Bézier curve, allowing an assessment of bathymetric uncertainty due to measurement error and survey detail on the derived groundwater fluxes compared with the fixed bathymetry models. Findings show that different bathymetry conceptualisations can result in very different mass balance components and hence process conceptualisations, despite equally good fits to observed data, potentially leading to poor management decisions for the wetlands. Model predictive uncertainty increases with the crudity of the bathymetry representation, however, approximations that capture the general shape of the wetland pond such as a power law or Bézier curve show only a small increase in prediction uncertainty compared to the full dGPS surveyed bathymetry, implying these may be sufficient for most modelling purposes.

1. Introduction

The importance of wetlands to biodiversity is now widely recognized (Murray et al., 2003) and there is growing recognition of the importance of groundwater to many of these systems. Indeed, the management and policy requirements for the protection of groundwater dependent ecosystems (GDEs) globally are an important issue. However, with a few notable exceptions, the groundwater

requirements of these ecosystems are not well understood (MacKay, 2006). Numerical models, of which water and solute balance models are examples, have become an indispensable decision tool in groundwater management (Sophocleous, 2000). Modelling of GDE and groundwater interactions allows the development and testing of our conceptual understanding of how these systems function and is perhaps a key research area that would benefit management by allowing the projection of GDE response to different magnitudes, rates and season of groundwater drawdown, as well as different climatic scenarios (Eamus and Freund, 2006).

Water balance methods are often not sufficiently accurate to estimate groundwater inflow, and hence environmental tracer methods have been used in combination with water balance

* Corresponding author at: Hydrology Group, School of Geographical Sciences, University of Bristol, University Road, Bristol BS8 1SS, UK. Tel.: +44 (0)117 928 8290; fax: +44 (0)117 928 7878.

E-mail address: mark.trigg@bristol.ac.uk (M.A. Trigg).

Nomenclature

A	wetland surface area (m ²)	$P_{0,1,2,3}$	Bézier control points coordinates (r, d)
c_g	groundwater inflow EC (mS/cm)	Q	surface & groundwater outflow (m ³ /day)
c	mean EC in wetland (mS/cm)	r	bathymetry radius (m)
c_p	mean precipitation EC (mS/cm)	r_0	max. bathymetry radius at d_0 (m)
c_Q	mean EC of pond outflow (mS/cm)	t	time (days)
c_s	mean surface water EC (mS/cm)	t_g	groundwater period parameter (days)
c_0	initial salt mass (kg)	V	pond volume (m ³)
d	wetland depth at deepest point (m)	α_p	precipitation factor
d_0	max. wetland depth (m)	α_E	evaporation factor
E	evaporation from pond (m/day)	α_g	groundwater input factor (m ²)
I_g	groundwater inflow (m ³ /day)	α_Q	groundwater output factor (m ² /day)
I_s	surface water inflow (m ³ /day)		
P	precipitation falling on wetland (m/day)		

methods to constrain the interactions between wetlands or lakes and groundwater. ²H and ¹⁸O have been applied widely to calculate groundwater inflow and outflow (Krabbenhoft et al., 1990; Hunt et al., 1996; Yehdegho et al., 1997; Gurrieri and Furniss, 2004) or surface water evaporation (Gibson et al., 1996; Yehdegho et al., 1997). Ion chemistry (including sodium, chloride and calcium) have also been used, both independently (Hayashi et al., 1998; Ferone and Devito, 2004; Heagle et al., 2007, 2013; Kizuka et al., 2011), and in combination with isotopic tracers (LaBaugh et al., 1997). Similarly, Corbett et al. (1997) and Schmidt et al. (2009) used point samplings in time of radon to estimate groundwater inflow. For highly transient systems, however, time series of tracer data are required to capture the dynamic nature of the water balance. In these systems, electrical conductivity has been used (e.g. Quinn et al., 2010) as it can be measured easily and remotely using sensors and data loggers. More recently, time-series of radon has also been used to analyse the transient dynamics of wetlands (Dimova and Burnett, 2011) and river bank infiltration (Gilfedder et al., 2013) over periods of several days.

All of the above mentioned tracers are interpreted by calculating a water and solute mass balance of the surface water body. These mass balances can be either applied in a steady-state or in a transient mode. Steady-state mass balance approaches do not require a detailed description of the bathymetry. However, in many cases steady-state approaches are not an appropriate description of the system and transient approaches need to be used. Observation data usually available to capture system dynamics are the changes in water depth and solute concentration over time. However, depth in itself is not sufficient to calculate in and outgoing water fluxes, and changes in water volumes over time are required. Similarly, water volumes are also required to calculate the changes in solute mass over time. However, volumes cannot be directly measured. The surface water area is also important because it controls evaporation losses and gas exchange processes. To link observations of depth to volume and surface area, the bathymetry of the system is required.

Despite the obvious importance of bathymetry, most solute and water balance studies provide scant information on how bathymetry was determined and the accuracy of the resulting depth-volume-area relationship e.g. Gurrieri and Furniss (2004), Dimova and Burnett (2011). In the absence of a detailed measured bathymetry, other studies assume a simple mathematical form for the bathymetry, which is parameterized with a small number of measurements of depth and area and/or volume, e.g. Castaneda and Angel Garcia-Vera (2008) and Hayashi and van der Kamp (2000). Minke et al. (2010) explore in some detail the basic bathymetric error in using these relationships compared to a detailed

survey, but do not quantify the implications for water and solute mass balance model results. Although uncertainty analyses on water and solute mass balances have been carried out in some cases (Gibson et al., 1996; Choi and Harvey, 2000), few studies consider how uncertainties in bathymetry may impact on estimated water balance components. The only study that we are aware of that specifically considers uncertainties introduced by errors in bathymetry is (McJannet et al., 2012), although in this case variations in lake volume were relatively small, and so uncertainty due to bathymetry was small relative to other model parameters. This might not be the case for shallower wetlands, where changes in pond area can be more pronounced, and hence the depth-volume relationship can become very non-linear.

In this paper, we use a solute and water balance approach to reconstruct the water balance of a shallow, groundwater dependent wetland pond over a period of six years. The solute and water balance is based on a time series of daily water depth and electrical conductivity measurements, and on measurements of wetland pond bathymetry obtained using dGPS and LiDAR survey. In particular, we examine how uncertainty in bathymetry affects the calculated water balance components by running the model with a range of bathymetry approximations.

2. Water and solute balances

The surface water balance for a pond can be expressed as:

$$\frac{dV}{dt} = I_s + I_g + PA - Q - EA \quad (1)$$

where V is the pond volume [L³], I_s is the surface water inflow rate [L³ T⁻¹], I_g is the groundwater inflow rate [L³ T⁻¹], Q is the combined surface water and groundwater outflow rate [L³ T⁻¹], P is the precipitation rate [L T⁻¹], E is the evaporation rate from the water surface [L T⁻¹], A is the surface water area [L²] and t is time [T]. V and A are typically inferred through water depth using equations describing the bathymetry.

The mass balance for a conservative solute can be written as:

$$\frac{dcV}{dt} = I_s c_s + I_g c_g + PA c_p - Q c_Q \quad (2)$$

where c is the mean concentration of tracer within the pond [M L⁻³], c_s , c_g and c_p are the mean concentrations in surface water inflow, groundwater inflow and precipitation, respectively, and c_Q is the mean outflow concentration. For isotopes and noble gases additional terms are required e.g. Krabbenhoft et al. (1990) and Cook et al. (2008).

Excluding any bathymetry parameters, Eqs. (1) and (2) include a total of 12 parameters, each of which may vary temporally. To reduce the complexity of the model it is common to make a number of simplifying assumptions depending on the characteristics of the wetland under consideration. Details of the study site are presented in the following section, and simplifying assumptions relevant to our water balance are as follows:

- (i) There is no surface stream runoff input, so that $I_s = 0$. This assumption is commonly used for areas with limited topographic relief and high infiltration rates. The study wetland and surrounding area have no permanent watercourses and surface runoff is very rare due to the sandy soils from the old sand dune systems.
- (ii) The wetland is perfectly mixed, so that $c_Q = c$. This is a common assumption for shallow and small wetlands. Measurements of spatial variation of EC across the study wetland show this is a reasonable assumption here.
- (iii) c_p and c_g are constant in time. This assumption has to be made in the absence of long term data series. However, the solute concentration in groundwater tends to be stable over time in natural systems. Since solute concentrations in rainfall are typically a small component of the solute mass balance the impact of assuming constant c_p is usually not significant.
- (iv) The groundwater input to the wetland is proportional to the mean rainfall over a period of time, t_g [T]. This allows the groundwater inflow to vary temporally, without increasing the number of model parameters significantly. By varying t_g , both highly dynamic systems (small t_g) and systems with constant inflow (large t_g) can be represented.
- (v) Groundwater outflow is proportional to the depth of water in the pond, d [L]. Similarly, this allows us to vary the groundwater outflow temporally, without increasing the number of model parameters significantly.

Ideally, the influence of these simplifying assumptions on water and solute balances should be assessed on a case by case basis. With these assumptions, the water volume and solute mass balance becomes:

$$\frac{dV}{dt} = \frac{\alpha_g}{t_g} \int_{t-t_g}^t P(t') dt' + \alpha_p PA - \alpha_Q d - \alpha_E EA \quad (3)$$

$$\frac{dcV}{dt} = \frac{\alpha_g}{t_g} \int_{t-t_g}^t P(t') dt' c_g + \alpha_p PA c_p - \alpha_Q dc \quad (4)$$

where α_g , α_Q , α_p , and α_E are constants of proportionality for groundwater inflow, outflow, precipitation and evaporation terms, respectively. α_g has units of L^2 , α_Q has units of $L^2 T^{-1}$, and α_p and α_E are dimensionless. α_g can be envisaged as the product of the catchment area and the fraction of precipitation contributing to recharge. Parameter α_p (dimensionless) is the ratio of the total volume of water added to the pond from precipitation, to the volume of precipitation which only falls directly on the pond. Values of α_p greater than one indicate localised wetland runoff input to the pond, whereas a value of one indicates only direct rainfall input to the pond water surface. The value of parameter α_p also includes the effect of any consistent differences between rainfall at a measurement point and that at the field site. Similarly, a value of $\alpha_E = 1$ reflects evaporative loss from the pond only, whereas values greater or less than one allow for differences between pan evaporation at measurement point and actual evaporation from the wetland (Winter, 1981). To allow for the fact that a wetland can experience strong evaporitic enrichment of solutes which are then stored in the dry sediments and then become remobilised in the next season

during filling, we introduce a starting salt mass c_0 as the final model parameter.

3. Site description

We have chosen to apply our methodology to a shallow, groundwater dependent, transient wetland pond in southern Australia (ForestrySA, 2005; Cook et al., 2008). It is typical of many hundreds of hectares of GDEs in the area (ForestrySA, 2005) and across Australia (Murray et al., 2003), and importantly for a modelling assessment such as required here, has multiple years of daily water level and electrical conductivity measurements. The wetland is located in the Honan Native Forest Reserve (NFR), approximately 16 km northwest of Mount Gambier, in the southeast of South Australia (Fig. 1). The reserve is 1030 hectares in size, and the topography consists of gently undulating dunes with wetlands occupying some of the depressions. The reserve contains 160 hectares of wetlands, and is the largest conserved area of native forest woodland and enclosed wetlands in this part of South Australia (ForestrySA, 2005).

The mean annual rainfall (1981–2010) of the area is 708 mm, and mean annual pan evaporation is approximately 1270 mm (source Mount Gambier airport – Station Number 026021). Most of the wetland ponds in the Honan NFR are less than 1 m in depth and vary greatly in size in response to seasonal or inter-annual variations in rainfall, and may dry completely in some years. The regional unconfined aquifer is in the Gambier Limestone, but within the reserve this is buried by up to 30 m of Aeolian sand deposits with interbedded clay lenses. Hydraulic head data suggest a fault to the south is acting as a barrier to regional groundwater flow and maintaining a higher water table in the vicinity of the reserve, thereby influencing the development of wetlands and aquatic communities. Groundwater salinity is mostly between 500 and 1000 mg/L total dissolved solids. No streams enter or leave the wetland, and for most years, there is no surface water inflow or outflow (Fig. 1). The direct surface catchment area of the wetland, estimated from LiDAR topography is approximately 150,000 m^2 . The boundary of the wetland can be clearly identified by the vegetation change from rushes and water lilies to a dense thicket of *Leptospermum continentale* and various eucalyptus species, which are the dominant vegetation type for the surrounding catchment area. There is no “willow ring” of riparian vegetation typical of North American prairies (van der Kamp and Hayashi, 2009), rather a continuous vegetated area away from the wetland. The wetland extent coincides with the maximum pond extent observed during the study period. Permeability of the surrounding sandy soils is high and therefore surface runoff is very rare. Groundwater levels fluctuate in response to seasonal variations in rainfall and evaporation, but generally indicate flow towards the wetland from the north and west. There is also some indication of flow through the wetland to the south and east, although large seasonal fluctuations and vertical gradients mean that a potentiometric surface is difficult to accurately define. Cook et al. (2008) measured radon activities within the wetland on three occasions in 2006 and estimated groundwater inflow rates using a radon mass balance. However, the transient nature of groundwater flow into and out of these wetlands remains to be fully understood.

Observations at the wetland commenced in 2006. At that time, much of southeastern Australia was undergoing drought, and between 2006 and 2010 the wetland dried out each summer. Mean annual rainfall between 2005 and 2008 was 676 mm, compared to a long-term mean of 708 mm (1981–2010). Typically, the wetland pond would begin to fill in June or July, reach a maximum depth and extent between September and November, and finally dry out by February or March. The wetland is surrounded by woody vegetation, and this boundary probably indicates the maximum

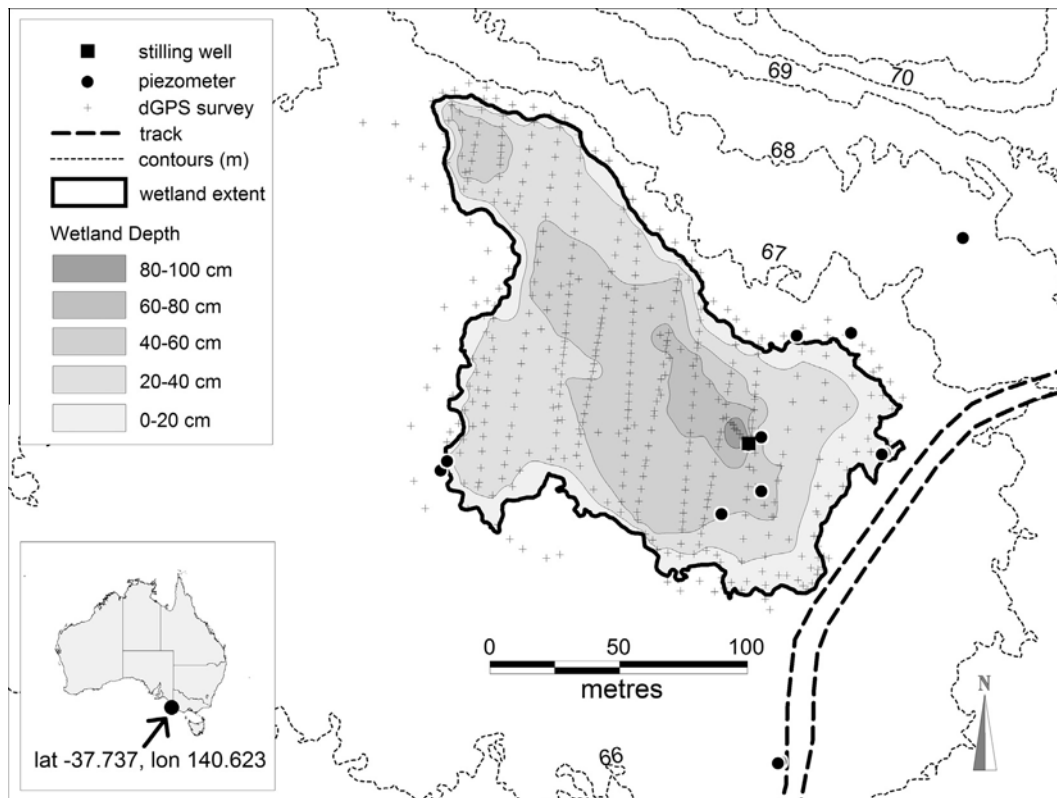


Fig. 1. Study area location map showing detailed wetland pond bathymetry (based on differential GPS survey) and surrounding topography contours (based on LiDAR data). Also shown are the piezometers (circle symbols) and stopping well (square symbol) for the level and EC loggers located near the deepest point in the wetland.

extent of regular inundation. The area enclosed by woody vegetation is 18,000 m², and the maximum depth of the wetland pond at this extent would be 0.65 m. Annual rainfall in 2010 and 2011 was 818 and 847 mm, respectively, and as a result of the increased rainfall, the wetland did not dry up during the 2010–2011 summer.

4. Methodology

Using the equations and assumptions outlined above, we estimate all water balance components for the wetland, although groundwater inflow and outflow are of particular interest. The tracer we employ in our approach is electrical conductivity as EC sensors and data loggers are readily available. Although, strictly speaking, electrical conductivity is not conservative, it may be used to represent the mass balance of the total dissolved ions, provided that (i) concentrations are sufficiently low, so that a linear relationship between EC and total dissolved ions can be assumed, and (ii) chemical reactions and ion exchange processes do not significantly alter the concentrations of the dominant ions. Salt mass and concentration are calculated by assuming that 1 mS/cm EC represents a dissolved salt concentration of 0.6 g/L.

We calibrate the parameters α_g , α_Q , α_p , α_E , c_0 , c_g , c_p , and t_g based on observations of c and d at our wetland, and P and E data obtained from a nearby meteorological station (Mt. Gambier). Measurements of d were made at the deepest point in the wetland, and a number of different approaches for estimating A and V were tested. Methods for describing how these parameters were obtained are described below.

4.1. Field sampling

The water level within the wetland pond has been measured since June 2006 by means of a stopping well (a piezometer within

the pond with screened interval above the land surface) equipped with a pressure transducer recording at hourly intervals (Fig. 1). Barometric pressure was measured and used to convert pressure to water level.

Electrical conductivity (EC) of the pond was measured on 29 occasions between May 2006 and September 2007. On seven occasions (24/5/06, 14/6/06, 25/7/06, 10/10/06, 18/7/07, 26/09/07 and 29/3/11), electrical conductivity was measured at between 20 and 60 locations within the pond, at half the pond depth (typically at 10–30 cm depth), with an EC electrode (WTW Ph/Cond 340i). In some locations three readings were taken at different depths, near surface, mid-depth and bed, to assess vertical variation in EC. An electrical conductivity sensor and logger was permanently installed in the pond in July 2008 by attaching it to the outside of the stopping well.

Fifteen shallow piezometers have been installed within the catchment. These piezometers range between 1.5 and 13.6 m in depth. Groundwater samples were collected from piezometers surrounding the pond after first purging three well volumes (Cook et al., 2008). Groundwater samples from the shallow perched aquifer were also obtained from 0.1 m diameter holes, drilled to between 0.8 and 1.2 m depth using a hand-auger. Immediately after drilling, the water in these holes was removed using a small submersible pump or bailer. The following day, water which had re-entered the holes was sampled and the holes were then back-filled. A total of 24 groundwater samples were thus obtained (24 May, 25 July and 9 October 2006), and analysed for EC and chloride concentration. Precipitation was collected between March 2007 and January 2008, and aggregated samples were analysed at approximately monthly intervals for chloride concentration. Daily rainfall and pan evaporation data for the entire study period was obtained from Mount Gambier airport (Station Number 026021), approximately 14 km due East. An evaporation pan and climate station were installed in the wetland area for a separate study

showed that the Mount Gambier airport station was a good analogue for the wetland site (daily rainfall correlation coefficient 0.95). Calculated pan coefficients for the wetland varied from 0.5 to 2 (7-day integrated measurements), with high values occurring in May through August when the wetland pond was filling and pond evaporation is likely enhanced by water heat release from the shallow waters and upward net ground heat flux. Due to this complex variation in calculated pan coefficient, we do not apply a specific pan coefficient to the evaporation data used. Rather it is implicitly incorporated in the model parameter applied to evaporation.

Surface elevations of the wetland and surrounding areas were obtained from 2 m interval airborne LiDAR data. The LiDAR survey was flown between 15 July and 15 August 2007 when the water depth in the wetland pond was between 30 and 47 cm. The data validation procedure from the survey determined a Root Mean Square (RMS) of 0.1 m relative to ground truth survey. After collection and post-processing to remove vegetation elevations, vertical accuracy of these data are typically 0.15–0.30 m. LiDAR can be used to collect a useful approximation of the bathymetry of shallow wetlands when water levels are low.

A dedicated, detailed differential GPS topographic survey of the wetland was carried out on 30 March 2011 when the wetland was dry, using a Trimble R8-3 GNSS RTK. Points were collected at 5–10 m spacing in an irregular grid pattern, with extra points recorded at obvious changes in slope and around the edge of the wetland to overlap with the LiDAR data. A total of 448 elevation points were collected over the 2 hectare survey area (Fig. 1).

4.2. Bathymetry representations

In order to examine the role of bathymetry on the results of the water and solute balance for our example wetland pond, different bathymetry formulations were used in the model. These included three fixed representations of varying accuracy; a constant area (**constant A**) assumption, a **LiDAR** derived relationship, and an interpolated **dGPS** survey derived relationship. The effect of representing the dGPS surveyed bathymetry using a curve fit rather than as an explicit bathymetry table is tested with a **power** curve fit (Hayashi and van der Kamp, 2000) and a **Bézier** curve fit (Bézier, 1968). Finally, the effect of uncertainty in the measurement of the dGPS bathymetry survey is tested by using parametrically defined envelopes of possible bathymetry Bézier curves. The parametric envelopes are constrained by the measurement uncertainty as well as using less survey points (i.e. to simulate an increased survey spacing) to define the bathymetry.

4.2.1. Fixed bathymetry representations

The constant area method is the crudest representation of the wetland bathymetry and uses a surface area equal to the full wetland extent ($\sim 21,000 \text{ m}^2$) that does not vary with wetland depth. This is the simplest method for representing the bathymetry and is included in this analysis for comparison with more typical bathymetry representations. In deep, steep-sided ponds this can be a valid assumption, but for shallow wetland ponds, actual open water surface area can vary greatly with depth, meaning this method can introduce considerable uncertainty into the modelling.

Digital terrain models, if available and of sufficiently highly resolved, can be used to calculate bathymetry. Numerous authors have used LiDAR technologies for this purpose (Lane and D'Amico, 2010; e.g. Huang et al., 2011). In the absence of a DEM, bathymetry can be calculated by contouring elevation measurement point data (Wilcox and Huertos, 2005; Cook et al., 2008). We used the LiDAR survey described in the field sampling section to derive the second fixed bathymetric relationship. For our most accurate bathymetry representation, we used the dGPS data. These data were then interpolated into a 0.5 m regular grid using 3D

analyst in ArcGIS based on the method of Hutchinson and Dowling (1991). Derived wetland bathymetries based on Constant Area, LiDAR and dGPS surveys are depicted in Fig. 2.

4.2.2. Parameterised bathymetry approximations

We use two mathematical approximations to provide an alternative parametric representation to the measured dGPS bathymetry relationship. These are the power law approach (O'Connor, 1989; Hayashi and van der Kamp, 2000; Brooks and Hayashi, 2002; Nilsson et al., 2008) and the Bézier curve (Bézier, 1968). The power law conveniently describes a wetland bathymetry using a single parameter and has been demonstrated as a sufficiently accurate approximation for many prairie wetlands (Hayashi and van der Kamp, 2000; Minke et al., 2010). The Bézier curve provides a greater range of volume–area–depth relationships than that the power law, at the expense of more parameters. The explicit formulation for the cubic Bézier curve applied in this paper is

$$f(x) = (1-x)^3 P_0 + 3(1-x)^2 x P_1 + 3(1-x)x^2 P_2 + x^3 P_3 \quad (5)$$

where P_0 , P_1 , P_2 and P_3 are the control points for the curve. The curve begins at P_0 and ends at P_3 , with P_1 and P_2 providing directional information that modifies the path of the curve between its beginning and end. The curve does not necessarily pass through P_1 and P_2 . The value of x varies from 0 to 1 and describes how far $f(x)$ is between P_0 and P_3 . Practical application for a curve in the two dimensional bathymetry plane requires Eq. (5) to be applied to the pond radius (r) and pond depth (d) axes of the control points independently. As with the power curve in Hayashi and van der Kamp (2000), the Bézier curve is rotated 360 degrees around a central point (the middle of the wetland pond) and the volume swept out by the curve provides a symmetrical bathymetry for the pond. Fig. 3a provides an example cubic Bézier curve with associated control points in the bathymetry space. The depth on the d axis is normalised by the maximum depth in the centre of the pond (d/d_0), and the symmetrical pond radius on the r axis is normalised by the maximum pond radius that reproduces the maximum pond extent area (r/r_0). Maximum depth and radius need to be chosen to encompass the bathymetry range expected in the model runs, and for this pond cover the area enclosed by non-wetland vegetation. Note that P_0 defines the centre of the wetland and P_3 defines the maximum extent and depth and are thus fixed. The maximum extent and depth are used to represent the final point constraining the end tangent of the Bézier bathymetry curve. Extreme wet conditions above this point involve extrapolation of the end tangent, much like other curve fit methods would. P_1 and P_2 however can vary parametrically for our purposes, with a value of r and d for each point resulting in a total of four parameters. Within the model, the resulting curve defines the area–depth relationship and numerical integration provides the volume–depth relationship.

The Bézier curve method includes all the curves possible with the Hayashi and van der Kamp (2000) method, but importantly for this assessment of bathymetry uncertainty also allows a much wider range of curves within the bathymetry space. In addition, this flexibility allows an accurate parametric representation of the multiple-slope Honan wetland bathymetry. Nine examples of the range of possible cubic Bézier curves within the bathymetry space are shown in Fig. 3b. Possible curves range from a simple straight slope representing a cone shaped pond, to concave and convex sloped shapes and also compound slope curves.

Bathymetries for the model using a power law and Bézier curve fitted by least squares error to the dGPS survey bathymetry allow us to assess the effect of approximating the surveyed bathymetry with a single parameter curve as well as one that allows a closer fit to the compound shape of the wetland pond (Fig. 4b). The power

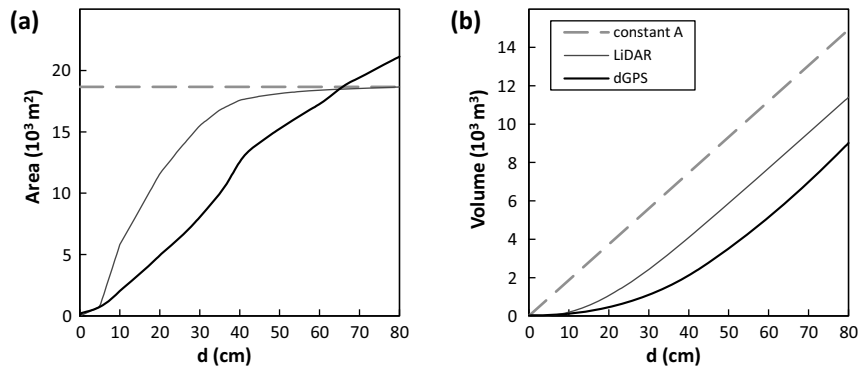


Fig. 2. Measured bathymetry, (a) area–depth relationship, and (b) volume–depth relationship.

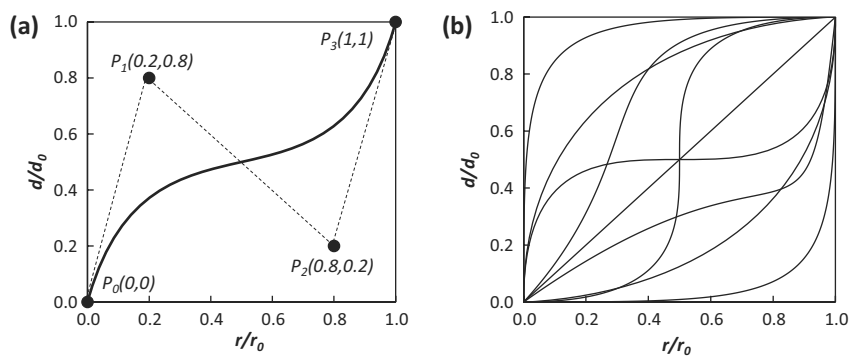


Fig. 3. Parametric bathymetry representation using a cubic Bézier curve rotated 360 degrees around the middle of the wetland, with volume swept out by the curve providing a symmetrical bathymetry for the wetland. (a) Typical cubic Bézier curve with control points and (b) examples of the range of possible cubic Bézier curves within the bathymetry space. The depth on the d axis is normalised by the maximum depth in the centre of the wetland (d/d_0), and the symmetrical wetland radius on the r axis is normalised by the wetland radius at maximum extent (r/r_0).

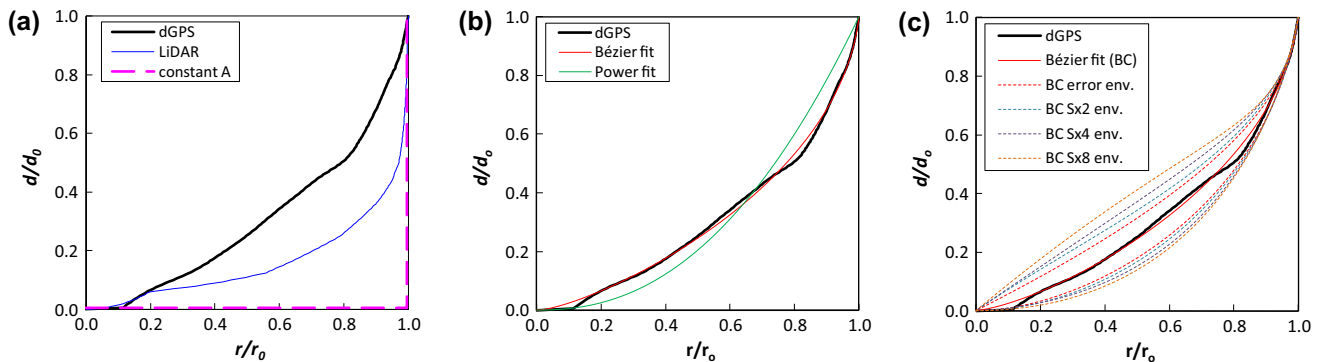


Fig. 4. Fixed and parameterised bathymetry models. The depth (measured at the centre of the wetland pond) on the d axis is normalised by the maximum depth (d/d_0), and the symmetrical pond radius on the r axis is normalised by the maximum pond radius at maximum extent (r/r_0). (a) For the surveyed bathymetries, LiDAR and dGPS, the curves are calculated from an equivalent area radius for the surveyed area at each depth. (b) Power law fit (exponent = 2.291) and Bézier curve fit (parameters in Table 3) to dGPS surveyed bathymetry. (c) Bézier curve fit envelopes showing range of possible curves when taking into account measurement error on the dGPS survey, and survey spacing. The Sx2 envelope represents two subsets with 50% of the original points, Sx4 four subsets with 25% of the points and Sx8 eight subsets with 12.5% of the points.

law fit exponent was 2.291 and the Bézier curve fit parameters are shown in Table 1.

4.2.3. Bathymetry uncertainty envelopes

Representing the bathymetry in the model using a Bézier parametric curve also allows us to explicitly represent uncertainties in our bathymetry by allowing the curve parameters to vary within a defined bathymetric envelope during the model runs. Setting the range over which the bathymetry parameters can vary is implemented by providing an upper and lower limit to the parameter ranges. We calculated this possible bathymetry envelope for

survey measurement error, and also for differing survey detail and implemented these within the model. Each envelope provides the upper and lower bounds of uncertainty on the bathymetry, with the actual bathymetry laying somewhere in between. The measurement error envelope is calculated by adding and subtracting an assumed measurement error of 0.05 m to the dGPS bathymetry survey points to provide the upper and lower bounds to the bathymetry envelope. Of practical interest it is also important to assess how detailed our survey might need to be to measure the bathymetry for modelling purposes. For this we simulate taking fewer survey points, effectively resulting in a larger survey

Table 1
Bézier curve bathymetry parameters for dGPS curve fit and bathymetry envelopes ranges.

Parameter	Units	Bézier curve (BC) fit	BC error env.	BC Sx2 env.	BC Sx4 env.	BC Sx8 env.
P_{1r}	m	12.1	0–33.8	0–40.6	0–49.6	0–57.3
P_{1d}	m	0	0	0	0	0
P_{2r}	m	76.8	76.8	76.8	76.8	76.8
P_{2d}	m	0.31	0.31–0.35	0.31–0.40	0.31–0.44	0.31–0.51

interval, by dividing the survey points into subsets and defining the bathymetry for each subset and finally using a summation of all these subsets (\pm measurement error) to define the upper and lower bathymetry envelopes. We did this for 2 subsets, 4 subsets and 8 subsets representing 50%, 25% and 12.5% of the survey points, abbreviated to Sx2, Sx4, Sx8 respectively in the rest of the paper. The original survey spacing was approximately 8 m, so the Sx2 point spacing is \sim 12 m, Sx4 is \sim 16 m, and Sx8 is \sim 24 m). Survey points were divided into 2 subsets by taking alternate points, and then into 4 subsets by taking alternate points of the first 2 subsets and so on for the 8 subsets. The derived envelopes and parameter ranges are shown in Fig. 4c and Table 1, and show a progressively increasing envelope space of possible bathymetries, reflecting the simulated coarser survey resolution.

4.3. Model Implementation and uncertainty analysis

Eqs. (3) and (4) were discretised to a daily timestep and coded in a Fortran model. The model reads in the rainfall and evaporation for the study period as input data and a file containing the parameter values together with a chosen bathymetry option. Bathymetry lookup tables derived from fixed bathymetry or the parameterised methods provide the relationship between wetland depth, surface area and volume for the model. The model outputs wetland depth, area, volume, and EC, as well as calculated fluxes. The model is automatically calibrated using the parameter estimation tools available in PEST (Doherty, 2010b), which uses a Gauss Marquardt Levenberg method to minimise a user defined objective function. The objective function for this study combined 2008 and 2009 observed depth and EC data and used 880 daily mean values of wetland depth and EC. These observed values were placed into four groups: depth and EC for each of 2008 and 2009. Each group was weighted by the inverse of the standard deviations of its values, which gives proportional weighting to each group. Standard deviations were 9.8 and 18.2 cm for 2008 and 2009 depth data, respectively; and 0.153 and 0.213 mS/cm for 2008 and 2009 EC data, respectively. The calibrated model is subsequently used to predict depth and EC for 2006–2007 and 2010–2011.

A summary of the parameters and the ranges used in the calibration are shown in Table 2. Parameter ranges for chloride concentration in groundwater and precipitation are based on the range of observed values. Parameter ranges for α_P , α_E , α_g , α_Q and t_g were deliberately chosen to be large. This PEST setup was then run for each bathymetry option. Typically, PEST required approximately 800 model runs to optimise the model parameters.

Predictive uncertainty analysis was undertaken using the PREDUNC suite implemented in PEST (Doherty, 2010b,a) which calculates the contribution of any model parameter to the uncertainty of a prediction. The theoretical basis for the analysis is given in (Moore and Doherty, 2005, 2006). The analysis assumes a linear relationship between parameter uncertainty and the uncertainty of the prediction. Several authors have shown that a linear uncertainty analysis can provide useful insights, even if applied to highly non-linear models (Dausman et al., 2010; Brunner et al., 2012).

For the bathymetry envelopes, it was only necessary to vary two of the four Bézier parameters to represent the full bathymetry

Table 2
Model input parameter ranges and starting values.

Parameter	Units	Min value	Max value	Start value
α_P	none	0.5	5.0	1.0
α_E	none	0.5	5.0	1.0
α_g	none	10,000	200,000	25,000
t_g	days	1	500	100
α_Q	none	0.1	10.0	1.0
c_0	kg	50	5000	750
c_P	mS/cm	0.05	0.1	0.07
c_g	mS/cm	0.1	4.0	1.0

space defined by the envelopes derived from the dGPS survey (P_{1r} and P_{2d}), see Table 1. We systematically sampled the parameter space defined by these two parameters within a Matlab script, running PEST for each resulting bathymetry (1681 runs), representing a total of approximately 1.3 million model runs. Results for all model runs from within a given envelope are accumulated to provide the range of possible results for that envelope. Thus the Sx2 results include the error envelope results, the Sx4 include both of the later and finally the Sx8 result includes all the results of all model runs.

5. Results

5.1. Observations

The observed EC of the groundwater varied between 0.59 and 4.51 mS/cm, but with most values between 1.1 and 2.2 mS/cm (mean 2.03 mS/cm), from the samples taken in 24 May, 25 July and 9 October 2006. The chloride concentration of monthly precipitation samples varied between 5.9 and 25.2 mg/L (mean 23 mg/L), with lower values recorded in the months that received greater rainfall volumes. The amount-weighted mean concentration was 10.1 mg/L, which is equal to the historical mean concentration measured in rainfall at Mount Gambier in 1974–75 by Blackburn and McLeod (1983). The mean electrical conductivity of precipitation was thus estimated using a TDS/Cl ratio of 2–3.5 for Mt Gambier (Blackburn and McLeod, 1983) to be approximately 0.03 mS/cm.

Variation in wetland water level and electrical conductivity between June 2006 and February 2012 are compared with variations in rainfall and pan evaporation at Mount Gambier airport (Fig. 5). Over this period, the wetland completely dried out each summer except for summer 2010/11. In both 2006 and 2007, the initial stages of filling were not recorded, and the wetland already contained water by the time pressure transducers were installed in late May and late June, respectively. However, in 2008 and 2009 the pond levels were below the stilling well depth of approximately 5 cm until early July. The wetland was dry by early December in 2006, but not until early February in the following years. In summer 2009/10 the wetland was dry for a period of only 2 months, and in 2010/11 the wetland did not dry out. The maximum water depth recorded over the four year period was 0.81 m.

The observed EC within the pond varied between 0.32 and 1.56 mS/cm over the period of measurement. EC is highest when the pond begins to fill, and decreases as the pond level increases.

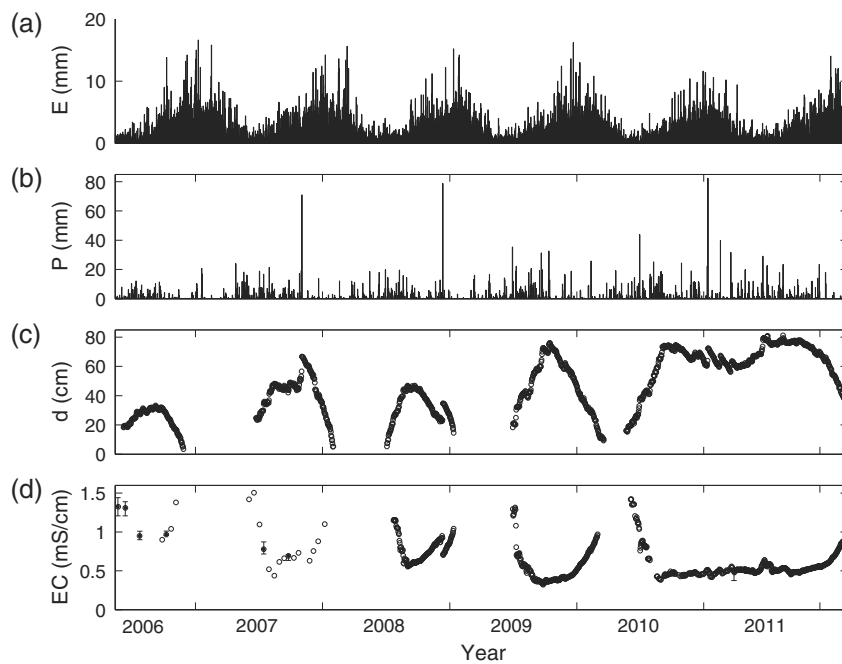


Fig. 5. (a) Evaporation, (b) precipitation, (c) wetland depth and (d) electrical conductivity measured at the deepest point of the wetland. (The sensor is located approximately 5 cm above the pond bottom, and so data is not recorded when the pond water depth is less than this.) A spatial sampling of EC across the wetland was undertaken on seven separate occasions (24/5/06, 14/6/06, 25/7/06, 10/10/06, 18/7/07, 26/9/07, 29/3/11) and the interquartile ranges are shown as error bars.

This suggests that initial filling of the wetland occurs due to groundwater inflow, but that rainfall input increases over time. The electrical conductivity then increases as the pond dries out. Sharp increases in depth and decreases in electrical conductivity were observed following large rainfall events (e.g. December 2008). The spatial variability of electrical conductivity within the wetland was measured on seven separate occasions and these ranges are plotted in Fig. 5d as error bars on those days. The spatial EC surveys showed a gentle EC gradient from the northeast to the southwest indicating there may be a throughflow across the wetland in this direction. There was no evidence of strong vertical variation in EC from the vertical sampling. Spatial variations, however, are very small compared to temporal fluctuations.

Calculation of the daily salt mass within the wetland from a wetland volume, derived from the measured depth and choice of bathymetry, then multiplied by the measured salt concentration, is highly dependent on the assumed bathymetry (Fig. 6). For example, in early September 2008, as the water level reached the maximum, the change in salt mass over time (dM/dt) is negative for all bathymetries, suggesting a loss of salt from the pond, and hence that outflow is occurring. However, the magnitude of dM/dt is much greater for the constant area bathymetry and least for the dGPS bathymetry. Early August shows a peak in dM/dt , likely due to the salt exchange process between surface water and near-surface sediments as last season's salt is mobilised. In mid-September 2008, the salinity increased while the water level remained relatively constant, and all bathymetries show a positive change in salt mass. This probably indicates groundwater flow into the wetland, but may also be partly due to salt exchange with the sediments. However, dM/dt is much greater for the dGPS and LiDAR bathymetries than for the constant area model which would result in a greater estimate of groundwater inflow at this time. During the subsequent decline in water level during October–November, all bathymetries show a decrease in mass over time, but in this case the constant area bathymetry gives the lowest rate of loss, suggesting a lower rate of outflow. Fig. 6 thus indicates the importance of bathymetry for water and solute mass balances.

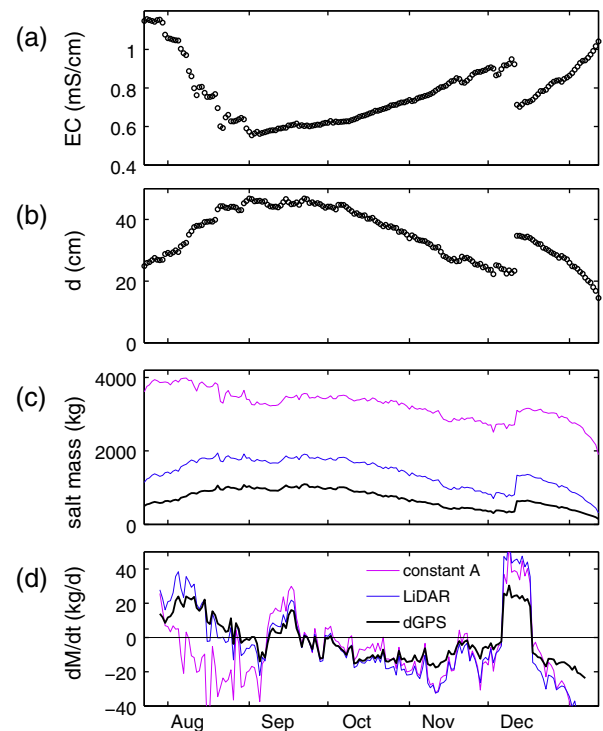


Fig. 6. (a) Wetland electrical conductivity and (b) depth data for 2008. Based on assumed bathymetries, calculated (c) salt mass and (d) change in salt mass over time are also shown. Data points in (d) show 11-day centred moving average of daily values. Salt mass is calculated by assuming that 1 mS/cm represents a dissolved salt concentration of 0.6 g/L.

5.2. Model calibration (2008–2009)

Model calibration covered the two wetland filling and drying cycles of 2008 and 2009 (Fig. 7, Table 3). All models provide a good

fit to the observed data, with the overall correlation coefficient for the combined objective function, r , of between 0.947 and 0.972. The best fit to the 2008 and 2009 data is provided by the constant area model and the worst is the LiDAR model.

Despite similar model fits to the observed EC and depth, the modelled water balance shows significant differences in daily P and E fluxes between bathymetry models (2008 results Fig. 8 and Table 4). Mean daily fluxes ranging from 23 to 68 m^3/d for P and 13–80 m^3/d for E . P and E fluxes are greatest for the constant area model, which has the greatest pond surface area of any of the models. There are also high variations in groundwater inflow (I_g) values between the models. Mean daily groundwater inflow rate varies between 21 and 54 m^3 , depending on the choice of bathymetry model, and outflow varies between 11 and 33 m^3 . The dGPS model has the smallest value of groundwater period (t_g) parameter (1 day), whereas the constant area model has the largest value (68 days). The LiDAR model has a t_g of 43 days. The small value of t_g for the dGPS model causes groundwater inflow to be highly episodic. The other models show a more seasonal pattern to groundwater discharge. Although the overall degree of fit was similar, the dGPS simulations have more pronounced short-term variability in depth and EC than observed in the data (Fig. 7).

The models using Bézier and power curve fit representations of the bathymetry show final optimised parameters and resulting fluxes very close to that of the dGPS model. However the Bézier curve fit model shows the closest similarity to the dGPS model and the power fit shows some pronounced divergences especially from the observed EC in 2008 (Fig. 7a).

As well as different mean flux values, the uncertainty in mean 2008 groundwater inflow and outflow for the constant area and LiDAR models is much wider than for the dGPS model (Fig. 9a and b). Again the uncertainties for the curve fit models are similar to that of the dGPS model. For the bathymetry envelopes, the inclusion of measurement error only results in a small increase in uncertainty over the dGPS baseline. For the reduced survey accuracy envelopes, the Sx2 model only shows a small increase in uncertainty, but for the Sx4 and Sx8 models this becomes much more pronounced. In addition to mean flux results for the optimum calibrated model runs and their uncertainty bounds (Fig. 9), it is also informative to plot the results for all the models runs within the bathymetric envelope (Fig. 10). Plots of the 2008 fluxes within the envelope parameter space shows that as the parameter envelope increases, a greater range of fluxes is possible, leading to an increasing uncertainty in the predictions. Notably, the groundwater outflow appears

Table 3
Final calibrated parameter values.

Parameter	Units	Constant A	LiDAR	dGPS	Bézier fit	Power fit
α_P	none	1.53	0.78	1.81	1.83	1.83
α_E	none	1.15	0.76	0.50	0.5	0.5
α_g	none	25,544	17,723	10,000	10,000	10,000
t_g	days	68	43	1	1	11
α_Q	none	0.92	0.33	1.05	1.07	1.01
C_0	kg	2420	742	330	654	843
C_P	mS/cm	0.10	0.05	0.05	0.05	0.08
C_g	mS/cm	0.23	0.30	1.15	1.19	1.02

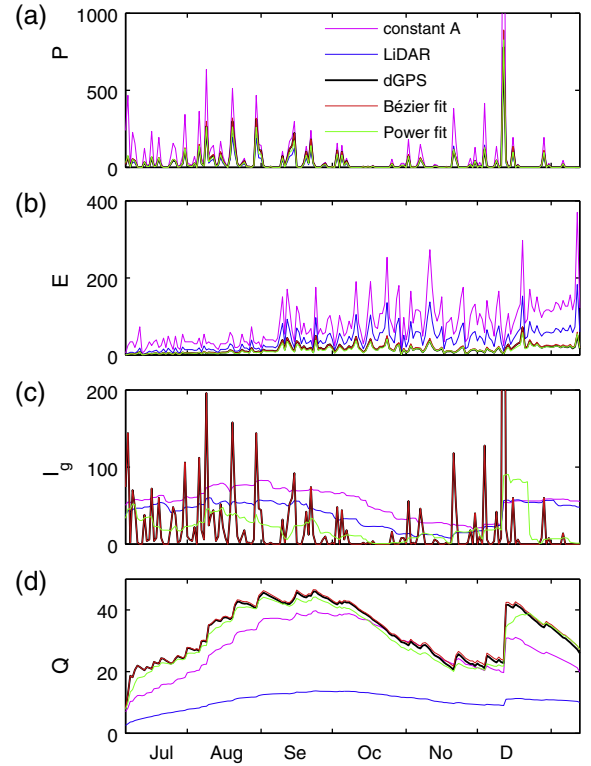


Fig. 8. Daily water balance fluxes (m^3/d) for 2008 for calibrated models. Note that precipitation and groundwater inflow fluxes in December 2008 exceed the data range of the vertical axes. Note, Bézier fit line coincides closely with the dGPS line.

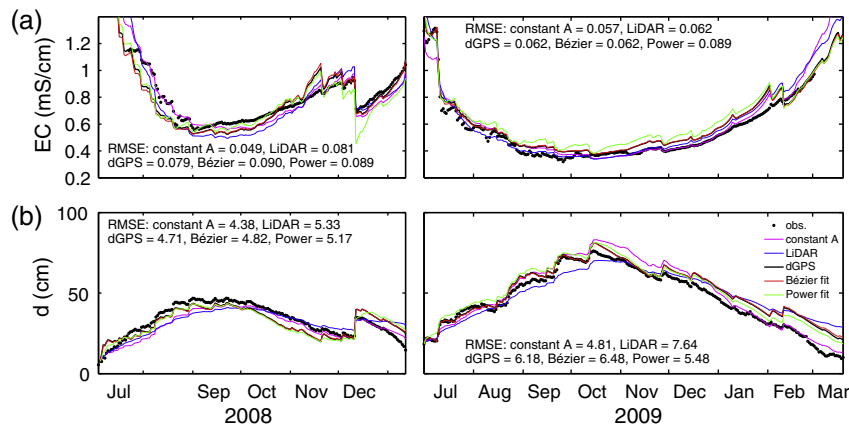


Fig. 7. Model calibration results and observations for 2008 and 2009 for the four different bathymetries. Overall objective function correlation coefficients (r) are: Constant Area = 0.972, LiDAR = 0.947, dGPS = 0.960, Bézier fit = 0.953 and power fit = 0.951. Individual RMSEs for each year and variable (same units as y-axis) are shown on each plot. Note, Bézier fit line coincides closely with the dGPS line.

Table 4
Modelled annual cycle mean daily volumetric fluxes 2008–2009 (m^3/day).

	Constant A	LiDAR	dGPS	Bézier fit	Power fit
2008					
P	68	23	30	32	27
E	80	40	15	16	13
I_g	54	39	21	21	22
Q	28	11	33	33	32
2009					
P	75	31	61	65	53
E	99	55	30	32	25
I_g	66	45	23	23	25
Q	46	16	54	55	52

to be generally more sensitive to the range of bathymetry parameters than the groundwater inflow. Equally good model fits can also be found in all the parameter envelope space unique to each envelope (i.e. none overlapping areas in Fig. 10c).

5.3. Model predictions (2006–2007)

Pond depth and EC were also simulated for 2006 and 2007, using the same parameter values. This enables comparison of

estimated wetland fluxes with those derived from radon data by Cook et al. (2008) (Fig. 9c–e and Table 5). Modelled groundwater inflows are mean values for the four day period up to and including the sampling date which is approximately the time period of the groundwater inflow rate estimated from the radon data. While the uncertainty associated with the radon measurements is hard to estimate, the samples show that the constant area and LiDAR fluxes are not even close. All other models show closer estimates of the 4 day flux relative to the radon based estimates. Again we see similar increases in uncertainty with cruder bathymetries, although more pronounced here than for the 2008 fluxes, presumably because these are four day means as opposed to mean annual values and are therefore more sensitive to model parameter values.

6. Discussion

Although there have been a number of water and solute balance studies of lakes and wetland ponds (e.g. Krabbenhoft et al., 1990; Gibson et al., 1996; Hunt et al., 1996; LaBaugh et al., 1997; Yehdegho et al., 1997; Hayashi et al., 1998; Gurrieri and Furniss, 2004; Heagle et al., 2007, 2013; Quinn et al., 2010), the use of long-term, high resolution (daily) data, such as employed in the

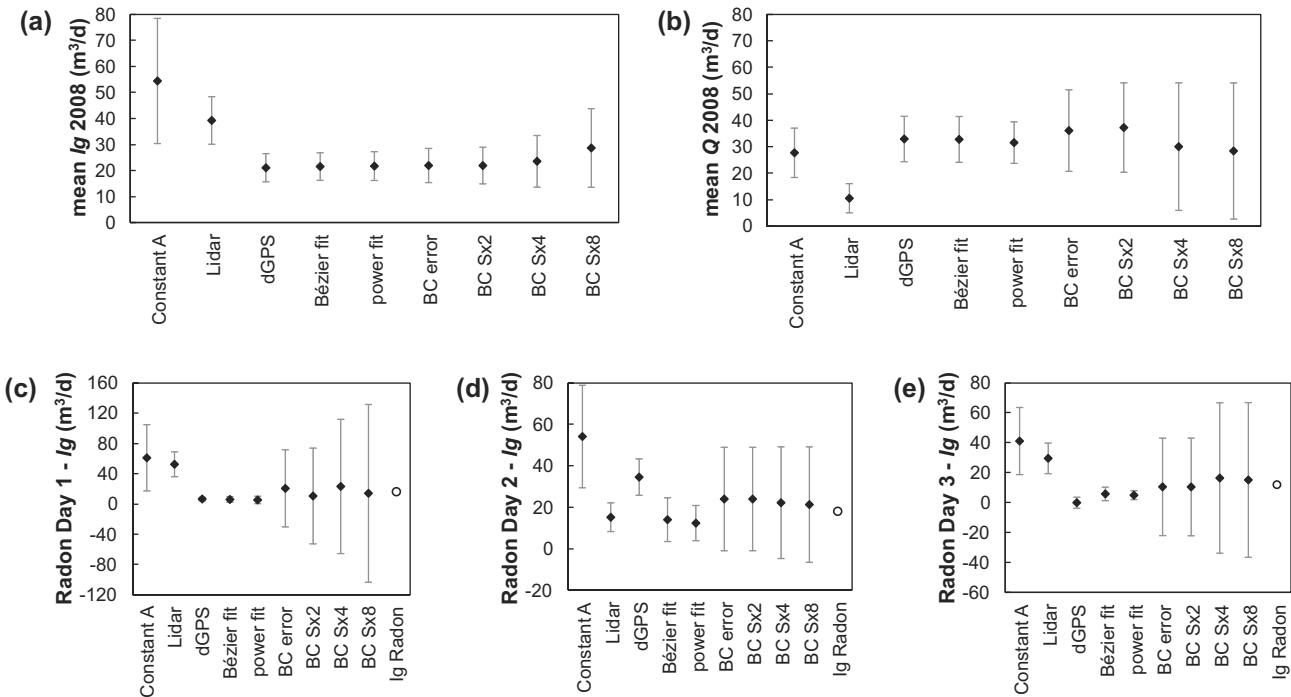


Fig. 9. (a) Mean daily groundwater inflow, I_g and (b) outflow Q predicted for 2008 for the different bathymetries. Error bars shows 99.7% (3σ) confidence intervals from generalised linear uncertainty analysis. (c) I_g Radon measurement day 1, four day mean (21–24 May 2006), (d) I_g Radon measurement day 2, four day mean (22–25 July 2006), (e) I_g Radon measurement day 3, four day mean (6–9 October 2006).

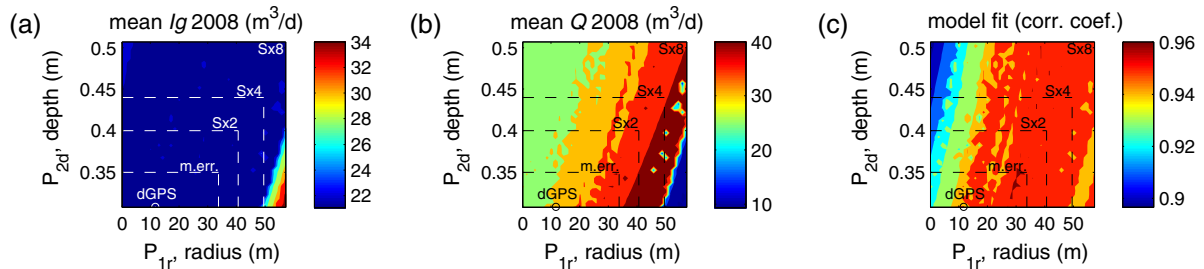


Fig. 10. Bezier curve bathymetry parameter space. (a) Mean groundwater inflow 2008. (b) Mean groundwater outflow 2008. (c) Model fit correlation coefficient. Bathymetry envelopes are shown by dashed labelled boxes and dGPS fit as a single labelled point.

Table 5

Comparison between modelled volumetric groundwater inflow fluxes (I_g) in 2006 and estimated fluxes based on radon data (Cook et al., 2008). Model values represent 99.7% (3σ) confidence intervals. Units are m^3/day .

	21–24 May	22–25 July	6–9 October
Constant area	17–105	29–79	19–64
LiDAR	36–69	8–22	19–40
dGPS	4–9	26–43	–4–4
Bézier fit	2–10	3–25	1–10
Power fit	0–10	4–21	2–8
Cook et al. (2008)	16	18	12

present study, is rare. The use of long-term, high resolution data allows model water balance components to be more accurately constrained than would be the case with a smaller number of observations. Over the wetland filling and drying cycles, different processes dominate at different times. For example, in our study, groundwater inflow dominates at the start of the cycle, and the pond is relatively saline. The next stage of filling is controlled by precipitation, and the salinity decreases. During the drying phase, the water balance is dominated by evaporation, and salinity increases again. The daily interval also captures the wetland response to both short-term highly transient processes such as direct rainfall on the wetland as well as the longer-term processes such as groundwater inflow/outflow.

Even with the deliberately simple nature of the model used, fits to the detailed calibration data and to data for non-calibration years for all models is good. This is despite very different conceptualisations of the bathymetry. While the fit to the observed water level and EC data is similar for all bathymetries, the actual optimised model parameters and water balance components are very dissimilar, resulting in very different conceptualisations of wetland system function. There is no surprise that very crude representations of bathymetry, such as the constant area approach, provide poor results when tested against measured fluxes. As shown here, a good model fit to calibration data is not the same as a good model. This variation in fluxes between models with equally good model fits reflects the non-unique nature of the modelling problem and serves as a note of caution regarding the use of these models in wetland areas where the underlying processes are not well understood.

Results of the model runs where curve fits represent the bathymetry show very similar results to the full dGPS surveyed bathymetry model. This indicates that these slightly cruder representations of the bathymetry have a minimal effect in the model predictive uncertainty. The implication is that as long as the approximate shape of the wetland pond is captured by the bathymetry in the model, then model uncertainty due to bathymetry should remain small. The effects of measurement error and reducing survey accuracy show potentially very different predicted fluxes and increasing uncertainty of predictions relative to the crudeness of the bathymetry representation. It should be noted that the uncertainties estimated by the model are only correct if the model assumptions, including bathymetry are correct. However, the relative differences estimated here do demonstrate the often “hidden” uncertainties associated with bathymetry assumptions and indeed that these may be as important as other parameters, at least for shallow wetlands.

Our study has shown that if the assumed bathymetry is wrong, the estimated water balance components can be in error. Whilst our shallow wetland case is probably tending towards the more extreme end of the bathymetric relationships, with a large surface area relative to volume, nonetheless it indicates that sensitivity testing should be applied to the bathymetric assumptions in water and solute balance models. “Soft” knowledge can help constrain the parameter space (Fienen et al., 2009) and reducing the number of possible non-unique model fits by careful choice of parameter

ranges applies as much to the bathymetric assumptions as for other more visible model parameters. Initial model results can be used to identify additional measurements which may further constrain the model or even identify missing processes. The use of additional tracers, such as radon and stable isotopes of water, also has the capability of constraining water and solute balance model structures further, as demonstrated here with the radon samples of Cook et al. (2008) and explored in more detail in a river system by McCallum et al. (2012).

Our model is based on a number of simplifying assumptions, and therefore it is likely that the “true” errors of the water balance components are underestimated (Doherty and Christensen, 2011). For example, transient water exchange with the riparian zone surrounding the pond, highlighted as important for North American prairie wetlands by van der Kamp and Hayashi (2009) is not represented explicitly as a process here and therefore will be incorporated implicitly within the other terms within the model. However, the prairie wetlands are underlain by low hydraulic conductivity glacial clays, limiting vertical movement of water, whereas here the wetland is underlain by old sand dunes on top of limestone bedrock and therefore lateral transfer to the riparian zone may be less important in this study wetland. While these other structural errors may introduce their own additional element of uncertainty (Doherty and Welter, 2010), the focus of this study is the increase in uncertainty when bathymetry assumptions are relaxed. Although the absolute errors may be underestimated, the relative errors reflect the importance of assumptions related to the bathymetry.

7. Conclusions

There is more model uncertainty associated with the assumptions regarding bathymetry for volume and solute balance models than is commonly acknowledged or explored. This bathymetric uncertainty, at least for shallow wetlands, could be as important as that due to other parameters within the model and therefore points to the need to constrain this often ignored model component. However, our study shows that as long as the approximate shape of the wetland pond is captured by the bathymetry in the model, then model uncertainty due to bathymetry remains relatively small.

Different bathymetry conceptualisations can result in very different mass balance components and hence process conceptualisations, despite potentially equally good fits to observed data. This has significant implications for the use of these models for the management of groundwater dependent ecosystems (GDEs) as it could lead to a completely erroneous understanding of wetland system function and incorrect model predictions and therefore lead to poor decisions. Far from being an intractable problem, different model conceptualisations can be used to identify measurements with which to test the models and help discriminate between the equifinality of the models.

The Bézier curve provides an appropriate and novel method of representing bathymetry parametrically and allows a large range of bathymetry shapes to be explored. Even though the Bézier curve allows a better curve fit to multi-slope bathymetries than the power law approach (Hayashi and van der Kamp, 2000), results of the two approaches are similar. This implies that unless a very close match to the real bathymetry is required, than the extra level of detail, and extra parameters, provided by the Bézier curve may be unnecessary.

Acknowledgements

Funding for this research was provided by the National Centre for Groundwater Research and Training, an Australian Government

initiative, supported by the Australian Research Council and the National Water Commission, by CSIRO Water for a Healthy Country and the Swiss National Foundation (AMBIZIONE grant PZ00P2_126415). Cameron Wood, Troy White, Enys Watt and Luisa Powell assisted with field sampling. Lawrence Burk conducted the demanding wetland topographic survey, and Nicolas White installed and maintained the depth and electrical conductivity loggers. LiDAR data was provided by South East Resource Information Centre (SERIC). The authors also wish to acknowledge assistance of John Doherty with application of the PEST model, Huade Guan for supplementary evaporation information, and Margaret Shanfield, Paul Bates and Luk Peeters for reviews of early manuscript drafts. Revision contributions by Mark Trigg were completed under funding provided by the Willis Research Network. We are also grateful for major constructive comments from our anonymous reviewers.

References

- Bézier, P.E., 1968. Use of NC at Renault for Car Body Design and Tooling. In: SAE Transactions, vol. 77, pp. 68–8.
- Blackburn, G., McLeod, S., 1983. Salinity of atmospheric precipitation in the Murry-Darling drainage division, Australia. *Aust. J. Soil Res.* 21 (4), 411–434.
- Brooks, R.T., Hayashi, M., 2002. Depth–area–volume and hydroperiod relationships of ephemeral (vernal) forest pools in southern New England. *Wetlands* 22 (2), 247–255.
- Brunner, P., Doherty, J., Simmons, C.T., 2012. Uncertainty assessment and implications for data acquisition in support of integrated hydrologic models. *Water Resour. Res.* 48, W07513. <http://dx.doi.org/10.1029/2011WR011342>.
- Castaneda, C., Angel Garcia-Vera, M., 2008. Water balance in the playa-lakes of an arid environment, Monegros, NE Spain. *Hydrogeol. J.* 16 (1), 87–102.
- Choi, J., Harvey, J.W., 2000. Quantifying time-varying ground-water discharge and recharge in wetlands of the northern Florida Everglades. *Wetlands* 20 (3), 500–511.
- Cook, P.G. et al., 2008. Groundwater inflow to a shallow, poorly-mixed wetland estimated from a mass balance of radon. *J. Hydrol.* 354 (1–4), 213–226.
- Corbett, D.R., Burnett, W.C., Cable, P.H., Clark, S.B., 1997. Radon tracing of groundwater input into Par Pond, Savannah River Site. *J. Hydrol.* 203 (1–4), 209–227.
- Dausman, A.M., Doherty, J., Langevin, C.D., Sukop, M.C., 2010. Quantifying data worth toward reducing predictive uncertainty. *Ground Water* 48 (5), 729–740.
- Dimova, N.T., Burnett, W.C., 2011. Evaluation of groundwater discharge into small lakes based on the temporal distribution of radon-222. *Limnol. Oceanogr.* 56 (2), 486–494.
- Doherty, J., 2010a. Methodologies and Software for PEST-Based Model Predictive Uncertainty Analysis. Watermark Numerical Computing, Brisbane, Australia.
- Doherty, J., 2010b. PEST: Model Independent Parameter Estimation. User Manual. Watermark Numerical Computing, Brisbane, Australia.
- Doherty, J., Christensen, S., 2011. Use of paired simple and complex models to reduce predictive bias and quantify uncertainty. *Water Resour. Res.* 47 (W12534), 2010. <http://dx.doi.org/10.1029/2011WR010763>.
- Doherty, J., Welter, D., 2010. A short exploration of structural noise. *Water Resour. Res.* 46, W05525. <http://dx.doi.org/10.1029/2009WR008377>.
- Eamus, D., Froend, R., 2006. Groundwater-dependent ecosystems: the where, what and why of GDEs. *Aust. J. Bot.* 54 (2), 91–96.
- Ferone, J.M., Devito, K.J., 2004. Shallow groundwater-surface water interactions in Pond-Peatland complexes along a Boreal Plains topographic gradient. *J. Hydrol.* 292 (1–4), 75–95.
- Fienn, M.N., Muffels, C.T., Hunt, R.J., 2009. On constraining pilot point calibration with regularization in PEST. *Ground Water* 47 (6), 835–844.
- ForestrySA, 2005. Honan Native Forest Reserve Revised Management Plan, Government of South Australia, ForestrySA, Mount Gambier.
- Gibson, J.J., Edwards, T.W.D., Prowse, T.D., 1996. Development and validation of an isotopic method for estimating lake evaporation. *Hydrol. Process.* 10 (10), 1369–1382.
- Gilfedder, B.S., Hofmann, H., Cartwright, I., 2013. Novel instruments for in situ continuous Rn-222 measurement in groundwater and the application to river bank infiltration. *Environ. Sci. Technol.* 47 (2), 993–1000.
- Guirri, J.T., Furniss, G., 2004. Estimation of groundwater exchange in alpine lakes using non-steady mass-balance methods. *J. Hydrol.* 297 (1–4), 187–208.
- Hayashi, M., van der Kamp, G., 2000. Simple equations to represent the volume–area–depth relations of shallow wetlands in small topographic depressions. *J. Hydrol.* 237 (1–2), 74–85.
- Hayashi, M., van der Kamp, G., Rudolph, D.L., 1998. Water and solute transfer between a prairie wetland and adjacent uplands, 2. Chloride cycle. *J. Hydrol.* 207 (1–2), 56–67.
- Heagle, D.J., Hayashi, M., van der Kamp, G., 2007. Use of solute mass balance to quantify geochemical processes in a prairie recharge wetland. *Wetlands* 27 (4), 806–818.
- Heagle, D., Hayashi, M., van der Kamp, G., 2013. Surface-subsurface salinity distribution and exchange in a closed-basin prairie wetland. *J. Hydrol.* 478, 1–14.
- Huang, S. et al., 2011. Demonstration of a conceptual model for using LiDAR to improve the estimation of floodwater mitigation potential of Prairie Pothole Region wetlands. *J. Hydrol.* 405 (3–4), 417–426.
- Hunt, R.J., Krabbenhoft, D.P., Anderson, M.P., 1996. Groundwater inflow measurements in wetland systems. *Water Resour. Res.* 32 (3), 495–507.
- Hutchinson, M.F., Dowling, T.L., 1991. A continental hydrological assessment of a new grid-based digital elevation model of Australia. *Hydrol. Process.* 5 (1), 45–58.
- Kizuka, T., Yamada, H., Hirano, T., 2011. Hydrological and chemical budgets of a mire pool formed on alluvial lowland of Hokkaido, northern Japan. *J. Hydrol.* 401 (1–2), 106–116.
- Krabbenhoft, D.P., Bowser, C.J., Anderson, M.P., Valley, J.W., 1990. Estimating groundwater exchange with Lakes. 1. The stable isotope mass balance method. *Water Resour. Res.* 26 (10), 2445–2453.
- LaBaugh, J.W. et al., 1997. Hydrological and chemical estimates of the water balance of a closed-basin lake in north central Minnesota. *Water Resour. Res.* 33 (12), 2799–2812.
- Lane, C.R., D'Amico, E., 2010. Calculating the ecosystem service of water storage in isolated wetlands using LiDAR in North Central Florida, USA. *Wetlands* 30 (5), 967–977.
- MacKay, H., 2006. Protection and management of groundwater-dependent ecosystems: emerging challenges and potential approaches for policy and management. *Aust. J. Bot.* 54 (2), 231–237.
- McCallum, J.L., Cook, P.G., Berhane, D., Rumpf, C., McMahon, G.A., 2012. Quantifying groundwater flows to streams using differential flow gaugings and water chemistry. *J. Hydrol.* 416, 118–132.
- Mcjannet, D., Wallace, J., Keen, R., Hawdon, A., Kemei, J., 2012. The filtering capacity of a tropical riverine wetland: I. Water balance. *Hydrol. Process.* 26 (1), 40–52.
- Minke, A.G., Westbrook, C.J., van der Kamp, G., 2010. Simplified volume–area–depth method for estimating water storage of prairie potholes. *Wetlands* 30 (3), 541–551.
- Moore, C., Doherty, J., 2005. Role of the calibration process in reducing model predictive error. *Water Resour. Res.* 41 (5), W05020. <http://dx.doi.org/10.1029/2004WR003501>.
- Moore, C., Doherty, J., 2006. The cost of uniqueness in groundwater model calibration. *Adv. Water Resour.* 29 (4), 605–623.
- Murray, B.R., Zeppel, M.J.B., Hose, G.C., Eamus, D., 2003. Groundwater-dependent ecosystems in Australia: It's more than just water for rivers. *Ecol. Manage. Restor.* 4 (2), 110–113.
- Nilsson, K.A., Ross, M.A., Trout, K.E., 2008. Analytic method to derive wetland stage-storage relationships using GIS areas. *J. Hydrol. Eng.* 13 (4), 278–282.
- Oconnor, D.J., 1989. Seasonal and long-term variations of dissolved solids in lakes and reservoirs. *J. Environ. Eng.-Asce* 115 (6), 1213–1234.
- Quinn, N.W.T., Ortega, R., Rahilly, P.J.A., Royer, C.W., 2010. Use of environmental sensors and sensor networks to develop water and salinity budgets for seasonal wetland real-time water quality management. *Environ. Model. Softw.* 25 (9), 1045–1058.
- Schmidt, A., Stringer, C.E., Haferkorn, U., Schubert, M., 2009. Quantification of groundwater discharge into lakes using radon-222 as naturally occurring tracer. *Environ. Geol.* 56 (5), 855–863.
- Sophocleous, M., 2000. From safe yield to sustainable development of water resources – the Kansas experience. *J. Hydrol.* 235 (1–2), 27–43.
- van der Kamp, G., Hayashi, M., 2009. Groundwater-wetland ecosystem interaction in the semiarid glaciated plains of North America. *Hydrogeol. J.* 17 (1), 203–214.
- Wilcox, C., Huertos, M.L., 2005. A simple, rapid method for mapping bathymetry of small wetland basins. *J. Hydrol.* 301 (1–4), 29–36.
- Winter, T.C., 1981. Uncertainties in estimating the water-balance of lakes. *Water Resour. Bull.* 17 (1), 82–115.
- Yehdegho, B., Rozanski, K., Zojer, H., Stichler, W., 1997. Interaction of dredging lakes with the adjacent groundwater field: an isotope study. *J. Hydrol.* 192 (1–4), 247–270.